Tuning the Electronic Band Gap of Oxygen-Bearing Cubic Zirconium Nitride: c-Zr3–x(N1–xOx)4

Teak Boyko, Andreas Zerr, Alexander Moewes

Tuning the Electronic Band Gap of Oxygen Bearing Cubic Zirconium Nitride: c-$Zr_{3-x}(N_{1-x}O_x)_4$

Teak D. Boyko,[*,†] Andreas Zerr,[‡] and Alexander Moewes[¶]

†*Canadian Light Source, University of Saskatchewan, Saskatoon, SK, S7N 2V3, Canada*

‡*LSPM, CNRS-UPR 3407, Université Sorbonne Paris Nord, 93430 Villetaneuse, France.*

¶*Department of Physics and Engineering Physics, University of Saskatchewan, Saskatoon, SK, S7N 2V3, Canada.*

E-mail: teak.boyko@lightsource.ca

Abstract

Group IVB nitrides with cubic Th_3P_4 structure have one of the highest known coordination numbers for a binary nitride. Current research has shown these materials have a narrow direct electronic band gap. However, there has been little research into the dependence of the electronic band gap on cation defects and whether tuning the electronic band gap is possible by controlling the level of substitutional oxygen without adversely affecting the overall electronic structure. The materials studied herein include an oxygen bearing defect zirconium nitride, c-$Zr_{2.86}(N_{0.88}O_{0.12})_4$, and oxygen free hafnium nitride, c-Hf_3N_4. We use a combination of soft x-ray spectroscopy and density functional theory to study the electronic structure and determine the electronic band gap as well as the exciton binding energy. Moreover, we extend our structural model to consider the dependence of the electronic band gap on oxygen substitution in c-Zr_3N_4. The results suggest that the electronic band gap can be precisely controlled

between 1.47 – 1.84 eV (674 – 844 nm) by adjusting the stoichiometry, without adversely affecting the electronic structure. The exciton binding energy of c-$Zr_{2.86}(N_{0.88}O_{0.12})_4$ is estimated to be 37 meV, and combined with both the direct narrow electronic band gap and stable electronic structure, demonstrates that this material is an ideal candidate to replace currently used materials, such as GaAs, in photovoltaic applications.

Keywords

Band Gap, Electronic Structure, Density Function Theory, Photovoltaic, Exciton, Nitride

Introduction

High-pressure materials research has yielded a multitude of advanced materials that are finding useful applications in industry.[1] These materials are typically semiconductors with highly desirable mechanical and electronic properties. In this study we focus on a binary nitride system that is known to have one of the highest coordination numbers, namely Th_3P_4 structured c-Zr_3N_4 and c-Hf_3N_4. The electronic structure has been extensively studied with theory[2–5] and the theoretical electronic band gap is widely accepted to be direct and in the range of 0.7 – 1.8 eV.[2] Experimentally, these materials are known to have a near infrared electronic band gap in the range of 1.6 – 1.8 eV,[6] making them a candidate to replace the widely used GaAs. However, there is still important discussion as to the effect of defects on the electronic structure and there are only a few experimental measurements of the electronic structure and band gap.[6,7]

Many high-pressure materials exhibit very promising mechanical properties. The Th_3P_4 structured group IVB cubic nitrides are no exception. Compressibility experiments suggust a bulk moduli of 250 GPa and 260 GPa for c-Zr_3N_4 and c-Hf_3N_4, respectively, with an expected hardness in the range of 30 GPa.[8] c-Zr_3N_4 and c-Hf_3N_4 were first synthesized in a Diamond Anvil Cell (DAC) at temperatures of 2500 – 3000 K and pressures of 15 – 18 GPa.[8]

Larger quantities of c-Zr_3N_4 have been synthesized using a multi-anvil cell, but the resultant product (studied here) was an oxygen bearing defect structure, c-$Zr_{2.86}(N_{0.88}O_{0.12})_4$.[9] The measured hardness of c-$Zr_{2.86}(N_{0.88}O_{0.12})_4$ was determined to be 12.0 GPa, but it is expected to be more than 30 GPa for dense samples;[8,9] thin films of c-Zr_3N_4 are known to have a hardness of 36 GPa.[7] In addition, the ease at which c-Zr_3N_4 can be produced has been improving[10,11] allowing for the production of large amounts of high quality material making c-Zr_3N_4 desirable for industrial electronic and mechanical applications.

It is clear that these cubic nitrides, with an oxygen bearing defect structure are not extraordinary with respect to their mechanical properties, but perhaps could be of interest with the possibility to tune the electronic band gap by introducing substitutional oxygen into the nitrogen sites through control of the synthesis conditions. The expected direct electronic band gap of these materials makes them very appealing for PhotoVoltaics (PV) and Light Emitting Diodes (LED). However, in addition to having a direct narrow electronic band gap, PVs require materials with good exciton mobility[12] as well as being resistant to the formation of mid-gap states from material defects.[13] Recent soft x-ray spectroscopy measurements determined the electonic band gap of c-$Zr_{2.86}(N_{0.88}O_{0.12})_4$ to be 1.6 $\pm$ 0.3 eV,[6] which agreed with previous optical measurements on c-Zr_3N_4 thin films,[7] however, the authors did not consider the effect of lattice defects and substitutional oxygen making it unclear if this material would be suitable for PVs.

In this study, we rigorously determine the electronic band gap of c-$Zr_{2.86}(N_{0.88}O_{0.12})_4$ using a similar method: X-ray Emission Spectroscopy (XES) and X-ray Absorption Spectroscopy (XAS), with full consideration of the lattice defects using Density Functional Theory (DFT). We study both the effect of defects on the electronic structure and estimate the exciton binding energy from the results of these DFT calculations. Extending this, we show that controlling the level of substitutional oxygen provides a means to tune the electronic band gap without adversely affecting the overall electronic structure. In addition, we use the same method to determine the electronic band gaps of c-Hf_3N_4 and reference materials, m-ZrO_2

and m-HfO_2, to study the nature of the surface oxides. Lastly, considering electronic band gap, exciton binding and the effect of lattice defects on the electronic structure, we explore whether c-$Zr_{2.86}(N_{0.88}O_{0.12})_4$ is a good candidate material for PVs.

Results and Discussion

Soft x-ray spectroscopy, XES and XAS, are powerful techniques to selectively study a material differentiating both on an elemental and site symmetry level. We use N 1s XAS/Kα XES (see Fig. 1) and O 1s XAS/Kα XES (see Fig. 3) measurements to study the local unoccupied/occupied Partial Density of States (PDOS) of the N p-states and the O p-states, respectively. The simulated N 1s XAS and N Kα XES of c-Hf_3N_4 agree very well with the corresponding measured spectra. There is one peak in the N 1s XAS of c-Hf_3N_4 at ≈ 401.7 eV that is not reproduced by the calculation, but this can be easily explained as being caused by the rock-salt structured δ-HfN, an expected synthesis by-product.[6] While we did not measure directly the reference δ-HfN, we show in Fig. 1 the reference spectra of δ-TiN and δ-ZrN. Considering the similarities between these N Kα XES spectra, the resonant XES measurement of c-Hf_3N_4 at 401.7 eV produces a peak at ≈ 392 eV and clearly shows that this feature in the XAS results from the δ-HfN present in the material. Turning to the more complicated c-$Zr_{2.65}(N_{0.88}O_{0.12})_4$ in Fig. 1, we also see equally good agreement between the measured and simulated spectra. Similarly, the simulated XES and XAS spectra of the reference materials, δ-TiN and δ-ZrN, have near perfect agreement with the measured spectra. This shows that these DFT calculations are successful in predicting the expected electronic structure and can be used to supplement the experimental data to reliably determine the electronic band gap.

The electronic band gap of novel materials is difficult to determine as the samples are rarely phase-pure. XES and XAS measurements combined with DFT calculations are an excellent tool to study the electronic band gap of these materials since they are relatively

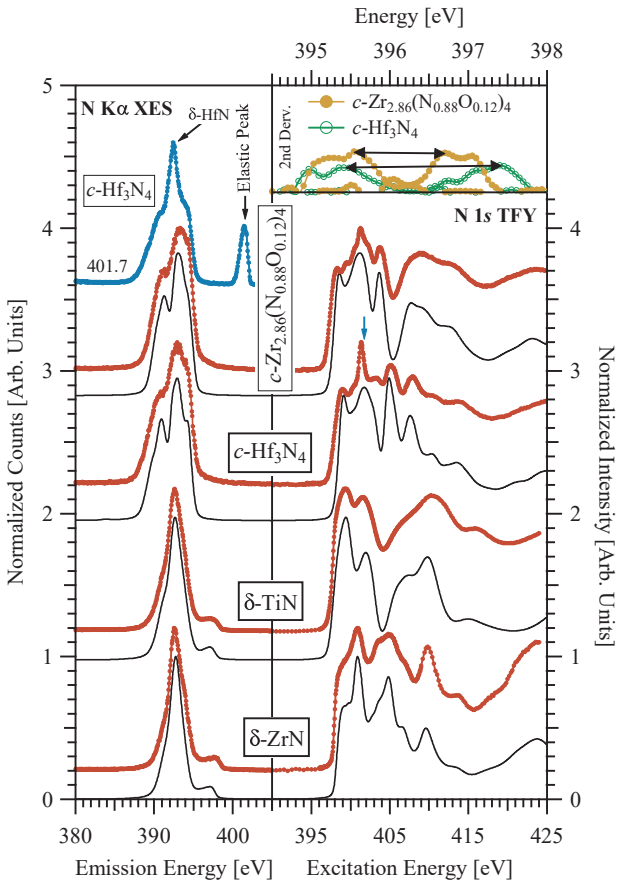

Figure 1: The measured N Kα XES and N 1s XAS spectra (red scatter) are compared to simulated spectra (solid lines). The excitation energy of resonant XES (blue scatter) is displayed to the left and corresponds to the arrow above the XAS spectra. The inset figure shows the second derivative of the measured spectra, with the band edges used to determine the electronic band gap indicated with arrows.

unaffected to contaminating phases with different elements or those in low concentration. Here, we use the N p-states, measured by N Kα XES and N 1s XAS, to determine the electronic band gap of oxygen bearing c-$Zr_{2.86}(N_{0.88}O_{0.12})_4$ and c-Hf_3N_4. This is advantageous since N p-states contribute to both the top of the Valence Band (VB) and the bottom of the Conduction Band (CB), as well the measurements are not affected by contaminating oxides. Table 1 shows all values associated with determining the electronic band gap including: XES to XAS energy separation, non-equivalent site splitting and core-hole shift. The former is obtained by taking the second derivative of the spectra, which is an established technique.[14] The latter two values need to be added to the first value thus providing the energy separation

between the VB and CB, specifically the electronic band gap. The final electronic band gap values of c-$Zr_{2.86}(N_{0.88}O_{0.12})_4$ and c-Hf_3N_4 are 1.75 ± 0.25 eV and 2.05 ± 0.25 eV, respectively. In addition, these values are close to our theoretical values, with c-Hf_3N_4 agreeing within experimental error. The slight disagreement for c-$Zr_{2.86}(N_{0.88}O_{0.12})_4$ is not unexpected considering the calculated electronic band gap values are highly dependent on lattice constants and the stoichiometry for the theoretical calculation is not exactly matching the experiment given the limitations of using a finite size crystal structure for DFT (c-$Zr_{2.875}(N_{0.875}O_{0.125})_4$ as a opposed to c-$Zr_{2.86}(N_{0.88}O_{0.12})_4$). These values also agree within experimental error when compared to the previous values from Ref. 6. The authors obtained these somewhat lower values because they did not consider any of the established corrections required when using XES and XAS to determine the electronic band gap nor the effect of defects on the XES and XAS measurements. However, the trend of the final values are similar and the narrow electronic band gap makes these materials suitable for PV devices.

Table 1: The electronic band gap values determined using the modified Becke-Johnson potential with the Local Density Approximation (E_G^{MBJ}) are compared to the experimentally measured values ($E_g^{Exp.}$) using the XES and XAS band separation (E_g^{SXS}) corrected for core hole screening and non-equivalent site splitting (ΔE)

Material	E_g^{MBJ} [eV]	E_g^{SXS} [eV]	ΔE [eV]	$E_g^{Exp.}$ [$\pm$0.25 eV]
m-ZrO_2	4.78	4.30	0.50	4.80
m-HfO_2	5.90	5.50	0.55	6.05
c-Zr_3N_4	1.37	—	—	—
c-$Zr_{2.86}(N_{0.88}O_{0.12})_4$	1.46	1.15	0.60	1.75
c-Hf_3N_4	1.97	2.00	0.05	2.05

Considering the success of the simulated spectra in reproducing the measured spectra regarding the N p-states, we turn to the calculated electronic structure, namely the electronic band structure and the PDOS. Figure 2 shows the element resolved PDOS for c-Zr_3N_4 and c-Hf_3N_4 as well as c-$Zr_{2.86}(N_{0.88}O_{0.12})_4$. Comparing the band structure, one can conclude that all materials have a direct electronic band gap. Inasmuch, the change between c-Zr_3N_4 and c-$Zr_{2.86}(N_{0.88}O_{0.12})_4$ is rather minimal, aside from the increase in the electronic band gap.

Turning now to the PDOS, the same conclusions are drawn and the presence of O p-states in the defect structure have a minimal effect on the N p-states. Furthermore, the O p-states are mainly situated at the bottom of the VB, but nearly equally contribute at the bottom of the CB, thereby playing a role in electronic band gap transitions. The lack of perturbation to the N p-states by including oxygen and Zr vacancies suggests c-$Zr_{2.86}(N_{0.88}O_{0.12})_4$ is an excellent candidate material for electronic band gap tuning; Fig. 2 shows the electronic band gap of c-$Zr_{3-x}(N_{1-x}O_x)_4$ (with x = 0.00 - 0.25) with both volume and force structural optimization using DFT. The trend shows that the electronic band gap can be precisely tuned between 1.47 – 1.84 eV through the control of substitutional oxygen without adversely affecting the electronic properties. The fact that the general electronic structure of c-$Zr_{3-x}(N_{1-x}O_x)_4$ appears to be largely unchanged going from a pristine structure to an oxygen bearing defect structure again strongly suggests that this material may be suitable for developing PV devices.

Important for PV applications, the exciton binding energy needs to be sufficient such that the free charge carriers do not disassociate quickly in the material. The band structure, combined with the relative static permeability, is used to determine the exciton binding energy for a Wannier-Mott type exciton.[15] Table 2 shows the exciton binding energies of c-Zr_3N_4, c-$Zr_{2.86}(N_{0.88}O_{0.12})_4$ and c-Hf_3N_4. The band structure is fit with parabolas at the VB maximum and CB minimum around the Γ-point to determine the effective masses. The exciton binding energy of these materials is determined to be much larger than that of the accepted value for GaAs, 4.2 ± 0.3 meV.[16] This combined with the ability to deposit c-$Zr_{2.86}(N_{0.88}O_{0.12})_4$ as thin films[7] and the potential to make large single crystals[11] yet again suggest these nitrides are good candidate materials for PV applications.

Turning now to the O p-states, we use O Kα XES and O 1s XAS measurements to study the arrangement of O atoms in the lattice and determine whether they likely subsitute nitrogen near the vacant zirconium sites. Figure 3 compares the simulated and measured O Kα XES and O 1s XAS of c-$Zr_{2.86}(N_{0.88}O_{0.12})_4$ and c-Hf_3N_4 as well as two reference materials

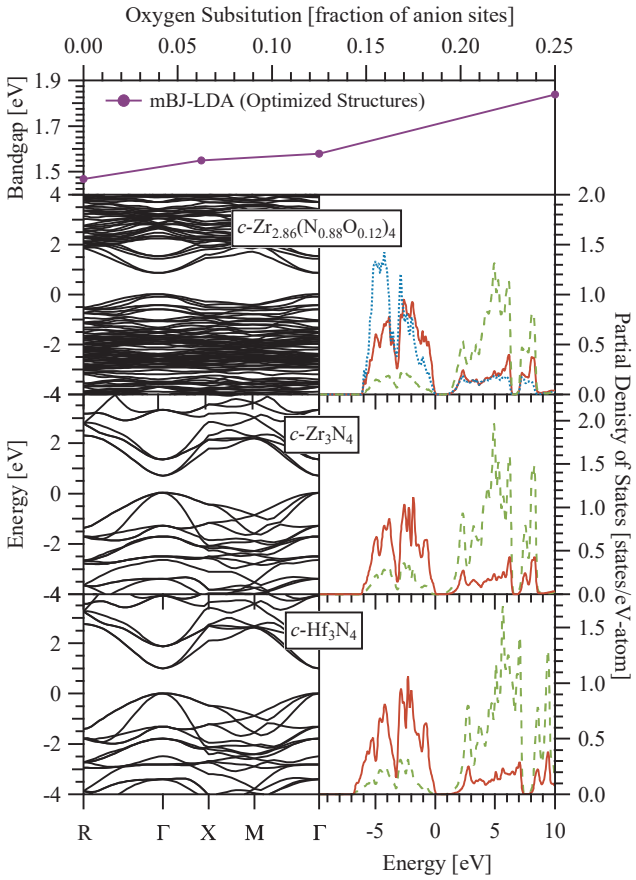

Figure 2: The electronic band structure (left), plotted using a simple cubic Brillouin zone, are compared. The density of states, including N p-states (red solid), Zr/Hf d-states (green long dash) and O p-states (blue short dash), are displayed to the right of the band structure. The upper panel shows the theoretical electronic band gap dependence on stoichiometry.

that represent an example of possible surface oxides, m-ZrO_2 and m-HfO_2. The simulated spectra reproduce the measured spectra quite well for the reference compounds. From this, we determine the electronic band gap of m-ZrO_2 and m-HfO_2 to be 4.80 ± 0.25 eV and 6.05 ± 0.25 eV, respectively. These values agree with our theoretical values within experimental error, however they are still widely debated in the literature.[17] While it appears clear that we have successfully simulated the spectra for m-ZrO_2 and m-HfO_2, the assessment for c-$Zr_{2.86}(N_{0.88}O_{0.12})_4$ is slightly more complicated. The pre-edge peak and general shape of the post edge of the measured O 1s XAS of c-$Zr_{2.86}(N_{0.88}O_{0.12})_4$ is well reproduced by the corresponding simulated spectra. Contrarily, the non-resonant O Kα XES spectra bears a strong resemblance to m-ZrO_2, but the resonant excitation shows something entirely differ-

Table 2: The parameters, relative static permittivity ($\epsilon(0)$), average effective hole mass (m_h^*), and average effective electron mass (m_e^*), determined from the band structure are used to calculate the average exciton binding energy ($E_{exciton}$)

Material	$\epsilon(0)$ [ϵ_0]	m_h^* [m_0]	m_e^* [m_0]	$E_{exciton}$ [meV]
c-Zr_3N_4	11.8603	1.19	0.45	32
c-$Zr_{2.86}(N_{0.88}O_{0.12})_4$	11.3379	1.07	0.53	37
c-Hf_3N_4	10.2689	1.34	0.45	43

ent. Exploiting the fact that zirconium oxides will have a much larger electronic band gap than c-$Zr_{2.86}(N_{0.88}O_{0.12})_4$, we excite on the first pre-edge peak, which should preferentially excite O atoms that are part of the c-$Zr_{2.86}(N_{0.88}O_{0.12})_4$ lattice. The resultant spectrum agrees very well with the simulated O Kα XES spectrum, showing a significant reduction of m-ZrO_2 character. This suggests that our model of c-$Zr_{2.86}(N_{0.88}O_{0.12})_4$ does exhibit the correct electronic structure of the O p-states. Above 535 eV the O 1s XAS spectrum of c-$Zr_{2.86}(N_{0.88}O_{0.12})_4$ sample shows significant contributions of other Zr oxides that are known to exist as bystander products in these materials.[6] Moreover, if we look at the O Kα XES and O 1s XAS of c-Hf_3N_4, we see the oxygen signal appears to originate entirely from an oxide similar to m-HfO_2. The resonant XES also does not change since there is likely only one oxide phase present. While our model may not be exact since we made some assumptions, it is sufficient to describe the electronic structure of c-$Zr_{2.86}(N_{0.88}O_{0.12})_4$. These results further support the notion that c-$Zr_{2.86}(N_{0.88}O_{0.12})_4$ has a very stable electronic structure with respect to lattice defects and oxygen substitution.

Conclusions

The electronic band gap of c-Zr_3N_4 and c-Hf_3N_4 are studied for the potential to tune the electronic band gap by controlling the level of substitutional oxygen in the crystal lattice. The electronic band gap is determined to be 1.75 eV and 2.05 eV for c-$Zr_{2.86}(N_{0.88}O_{0.12})_4$ and c-Hf_3N_4, respectively. The calculated electronic band gap values for c-$Zr_{2.86}(N_{0.88}O_{0.12})_4$

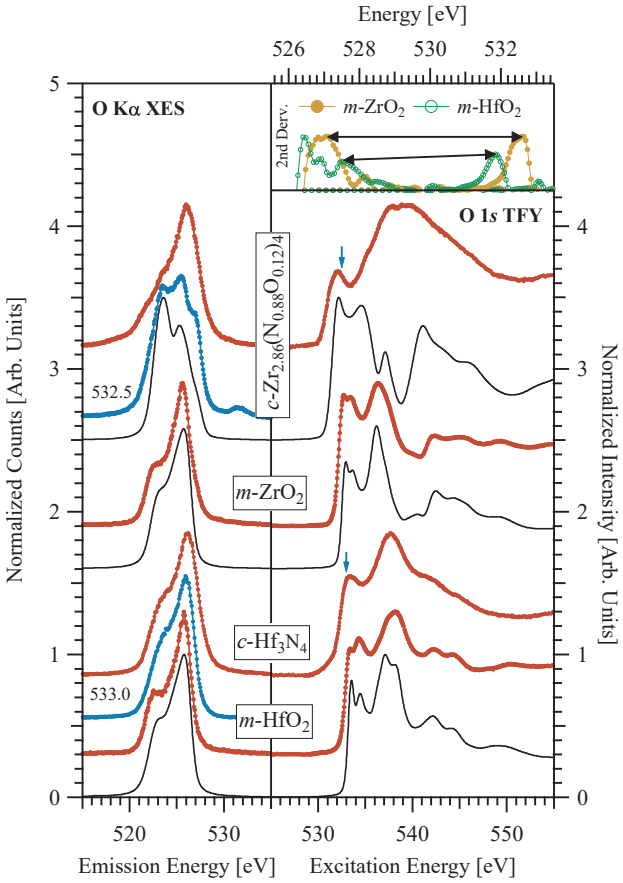

Figure 3: The measured O Kα XES and O 1s XAS spectra (red scatter) are compared to simulated spectra (solid lines). The excitation energy of resonant XES (blue scatter) is displayed to the left and corresponds to the arrow above the XAS spectra. The inset figure shows the second derivative of the measured spectra, with the band edges used to determine the electronic band gap indicated with arrows.

and c-Hf_3N_4 are 1.46 and 1.97 eV, respectively. The theoretical exciton binding energy is determined to range between 32 – 43 meV for Th_3P_4 structured cubic nitrides. Further theoretical study also shows that the electronic band gap of c-$Zr_{3-x}(N_{1-x}O_x)_4$ can be tuned precisely between 1.47 – 1.84 eV by controlling the amount of oxygen substitution from x = 0 to 0.25 during synthesis, without strongly affecting electronic structure or the exciton binding energy. Considering that these materials have three important qualities required for PV applications: (1) a direct narrow electronic band gap, a larger exciton binding energy, and a stable electronic structure with respect to lattice defects, they are good candidate materials to replace GaAs in modern photovoltaic devices.

Methods

Spectroscopy measurements probing the electronic structure, XES and XAS, were performed at Beamline 8.0.1[18] at the Advanced Light Source (Berkeley, CA) and the SGM beamline[19] at the Canadian Light Source (Saskatoon, SK), respectively. The XAS spectra were recorded using a micro-channel plate detector and the XES spectra were recorded using the SXF spectrometer at the corresponding beamlines. The samples were measured in a UHV environment for all XES and XAS. The powder reference samples (m-ZrO_2 and m-HfO_2) were pressed into indium foil (surface scraped clean) and affixed to the sample plate with carbon tape. The solid polycrystalline reference samples (δ-TiN and δ-ZrN) we affixed directly to the sample plate with carbon tape. The samples, c-Hf_4N_4 and c-$Zr_{2.86}(N_{0.88}O_{0.12})_4$, were encased in epoxy from previous measurements. These were affixed to the sample plate with carbon tape. The measured XES and XAS spectra were all calibrated with reference materials. The N K-edge spectra were calibrated using hexagonal BN (h-BN), using the two most prominent peaks near the band gap with the assigned values of 394.4 eV for XES and 402.1 eV for XAS, respectively. The O K-edge spectra were calibrated with BGO ($Bi_4Ge_3O_{12}$) using the two most prominent peaks near the band gap with the assigned values of 526.4 eV and 532.7 eV for XES and XAS spectra, respectively.[20] All data were normalized using the drain current from a Au mesh upstream of the sample chamber. A linear sloping background was subtracted from the XAS spectra, as this is caused by other non-resonant fluorescent lines.

The electronic structure calculations used the WIEN2k DFT calculation package (ver. 17.1).[21] The XES and XAS simulations utilized the calculated PDOS and applied the radial transition probability, non-equivalent crystallographic site considerations, corehole screening, and lifetime broadening. Importantly, the non-equivalent site splitting is determined from the DFT calculations and used to correct the nominal experimental electronic band gap values. In addition, the corehole screening is determined from these calculations and added to produce the final electronic band gap value. The theoretical band gap calculations use

the LDA with a modified potential from Becke and Johnson (mBJ-LDA),[22] which is known to accurately determine the electronic band gap of *sp* semiconductors. All of the similuated spectra use the GGA-PBE[23] functional.

The DFT calculations for the binary materials – which include: δ-$TiN_{0.98}$, δ-$ZrN_{0.97-1.00}$, m-ZrO_2, m-HfO_2, c-Zr_3N_4, and c-Hf_3N_4 – simply make use of the experimentally measured structure in Table 3. The two monoclinic reference oxides were purchased from Alpha Aesar, 11141 Zirconium(IV) oxide (99.978%) and 45483 Hafnium(IV) oxide (99.995%), as micro-crystalline powders. Two cubic mononitride samples were selected, δ-TiN and δ-ZrN, and procured from an industrial source with an expected stoichiometry of nearly 1:1. However, we independently measured the lattice constants and inferred the stoichiometry,[24,25] listed in Table 3, to be δ-$TiN_{0.98}$ and δ-$ZrN_{0.97-1.00}$. This near 1:1 stoichiometry suggests we do not need to consider the effect of vacancies in the structure used to simulate the x-ray spectroscopy since this will likely not be within the detection limit of the measurements. The k-mesh was chosen such that the total energy converged within 0.0001 Rydberg. The energy cutoff of core electrons was fixed at -6.0 Rydberg; additional details including k-mesh and RMT sizes are in Table S1. All other parameters we left as the default. The synthesis and structural details for c-Zr_3N_4 and c-Hf_3N_4 can be found in Ref. 8, here we make use of the measured structure for the DFT calculations.

In general, the structure of c-Zr_3N_4 and c-Hf_3N_4 can easily be described as they have a cubic lattice with only two unique crystallographic sites, one for the cation and one for the anion.[8] However, the oxygen bearing defect c-$Zr_{3-x}(N_{1-x}O_x)_4$ is more complicated and one needs to distribute both Zr vacancies and substitutional O atoms into the crystal lattice.[9] The authors of Ref. 9 suggest there is no evidence of ordering of the oxygen atoms and therefore we adopt a uniformly distributed model in our theoretical calculatons. We make the following assumptions: (1) the Zr vacancies will be uniformly distributed with as much separation between vacancies as possible and (2) the oxygen substitutions will occur around the Zr vacancy sites as to achieve local charge neutrality. A similar stoichiometry to c-

Table 3: Measured crystal structures used for DFT calculations

Material	Spacegroup	Lattice Constants	Source
δ-$TiN_{0.98}$	$Fm\bar{3}m$ (No. 225)	$a = 4.2401(7)$ Å	This work.
δ-$ZrN_{0.97-1.00}$	$Fm\bar{3}m$ (No. 225)	$a = 4.5752(7)$ Å	This work.
m-ZrO_2	$P2_1/c$ (No. 14)	$a = 5.145$ Å $b = 5.2075$ Å $c = 5.3107$ Å $\beta = 99.23°$	Ref. 26
m-HfO_2	$P2_1/c$ (No. 14)	$a = 5.1196$ Å $b = 5.1722$ Å $c = 5.2948$ Å $\beta = 99.18°$	Ref. 27
c-Zr_3N_4	$I\bar{4}3d$ (No. 220)	$a = 6.740(6)$ Å	Ref. 8
c-Hf_3N_4	$I\bar{4}3d$ (No. 220)	$a = 6.701(6)$ Å	Ref. 8

$Zr_{2.86}(N_{0.88}O_{0.12})_4$ is achieved by making a $2 \times 2 \times 2$ supercell. The resultant compound, c-$Zr_{2.875}(N_{0.875}O_{0.125})_4$, retains the body-centred symmetry and thereby significantly simplifies the calculation making XES and XAS simulations feasible. The substitution is distributed over all vacancies, which is 4 O atoms per vacancy with the longest Zr-O bonds chosen. The detailed structural parameters can be found in Table S2. We do not distinguish between c-$Zr_{2.86}(N_{0.88}O_{0.12})_4$ and c-$Zr_{2.875}(N_{0.875}O_{0.125})_4$, referring only to c-$Zr_{2.86}(N_{0.88}O_{0.12})_4$, which is very close to the experimental composition. The calculation proceeded with RMT sizes of 2.19, 1.87 and 1.93 for Zr, O and N, respectively. The k-mesh used was $5 \times 5 \times 5$, which provided sufficient energy convergence of 0.0001 Rydberg or better. The energy cutoff of core electrons was fixed at -6.0 Rydberg.

In order to extend to theoretical results beyond the material sample, c-$Zr_{2.86}(N_{0.88}O_{0.12})_4$, we assemble 4 theoretical structures for c-$Zr_{3-x}(N_{1-x}O_x)_4$ with $x = 0$, 0.0625, 0.125 and 0.25. These were created by making a $2 \times 2 \times 2$ supercell, with vacancies placed as indicated in Table S3 and the same procedure to substitute the N atoms with O as discussed above.

The structures were then volume optimized, with isotropic volume changes, and the atomic coordinates forced optimized simultaneously. The complexity of the structures makes listing all atomic coordinates problematic and the authors should be contacted to obtain detailed structures.

The calculation of the exciton binding energy is accomplished by collecting the following data: 1) The relative permittivity at zero photon energy from the calculation of the permittivity plots using DFT and 2) the effective mass extracted from the electron band structure. Since the effective mass of a hole or an electron depends on the dispersion direction we compute a geometric average of all possible dispersion directions and use that as the effective mass. Table S4 shows the effective masses calculated from the electron band structure. The exciton binding energy is then calculated using equation 1, where R_y is the Rydberg constant and m_e^*, m_h^*, $\epsilon(0)$ are the average effective electron mass, average effective hole mass and relative static permittivity, respectively. The effective masses are calculated using the approximation in equation 2.

$$E_{exciton} = \frac{m_e^* m_h^*}{(m_e^* + m_h^*) m_0 \epsilon(0)^2} R_y \tag{1}$$

$$E(\mathbf{k}) = E(0) + \frac{\hbar^2 \mathbf{k}^2}{2m*} \tag{2}$$

Acknowledgement

This research used resources of the Advanced Light Source, a U.S. DOE Office of Science User Facility under contract no. DE-AC02-05CH11231. Part or all of the research described in this paper was performed at the Canadian Light Source, a national research facility of the University of Saskatchewan, which is supported by the Canada Foundation for Innovation (CFI), the Natural Sciences and Engineering Research Council (NSERC), the National Research Council (NRC), the Canadian Institutes of Health Research (CIHR),

the Government of Saskatchewan, and the University of Saskatchewan. This research was enabled in part by support provided by Westgrid (www.westgrid.ca) and Compute Canada (www.computecanada.ca).

Supporting Information Available

The following files are available free of charge.

- Group_IV_Nitrides_AMI_SI.pdf: Details of theoretical structures and effective mass calculations.

References

(1) Zerr, A.; Riedel, R.; Sekine, T.; Lowther, J. E.; Ching, W. Y.; Tanaka, I. Recent Advances in New Hard High-Pressure Nitrides. *Adv. Mater.* **2006**, *18*, 2933–2948.

(2) Kroll, P. Hafnium Nitride with Thorium Phosphide Structure: Physical Properties and an Assessment of the Hf-N, Zr-N, and Ti-N Phase Diagrams at High Pressures and Temperatures. *Phys. Rev. Lett.* **2003**, *90*, 125501.

(3) Mattesini, M.; Ahuja, R.; Johansson, B. Cubic Hf_3N_4 and Zr_3N_4: A class of hard materials. *Phys. Rev. B* **2003**, *68*, 184108.

(4) Xu, M.; Wang, S.; Yin, G.; Li, J.; Zheng, Y.; Chen, L. Optical properties of cubic Ti_3N_4, Zr_3N_4, and Hf_3N_4. *Appl. Phys. Lett.* **2006**, *89*, 151908.

(5) Chihi, T.; Fatmi, M.; Ghebouli, B.; Guemmaz, M. Theoretical prediction of the structural, elastic, electronic and optical properties of Zr_3N_4 and Hf_3N_4 compounds. *Solid State Sci.* **2011**, *13*, 1414–1419.

(6) Yablonskikh, M.; Dzivenko, D.; Bourguille, J.; Riedel, R.; Magnano, E.; Parmigiani, F.; Zerr, A. Electronic structure and band gap of oxygen bear c-Zr_3N_4 and c-Hf_3N_4 by soft X-ray spectroscopy. *Phys. Status Solidi A* **2014**, *211*, 835–842.

(7) Chhowalla, M.; Unalan, H. E. Thin films of hard cubic Zr_3N_4 stabilized by stress. *Nat. Mater.* **2005**, *4*, 317–322.

(8) Zerr, A.; Miehe, G.; Riedel, R. Synthesis of cubic zirconium and halfnium nitride having Th_3P_4 structure. *Nat. Mater.* **2003**, *2*, 185–189.

(9) Dzivenko, D. A.; Zerr, A.; K, B. V.; Miche, G.; Li, J.; Thybusch, B.; Brötz, H.; Fueß, H.; Brey, G.; Riedel, R. High-Pressure Multianvil Synthesis and Structure Refinement of Oxygen-Bearing Cubic Zirconium(IV) Nitride. *Adv. Mater.* **2007**, *19*, 1869–1873.

(10) Dzivenko, D.; Zerr, A.; Miehe, G.; Riedel, R. Synthesis and properties of oxygen-bearing c-Zr_3N_4 and c-Hf_3N_4. *J. Alloy. Compd.* **2009**, *480*, 46–49.

(11) Taniguchi, T.; Dzivenko, D.; Riedel, R.; Chauveau, T.; Zerr, A. Synthesis of cubic zirconium(IV) nitride, c-Zr_3N_4, in the 6-8 GPa pressure region. *Ceram. Int.* **2019**, *45*, 20028–20032.

(12) Kuhar, K.; Pandey, M.; Thygesen, K. S.; Jacobsen, K. W. High-Throughput Computational Assessment of Previously Synthesized Semiconductors for Photovoltaic and Photoelectrochemical Devices. *ACS Energy Letters* **2018**, *3*, 436–446.

(13) Shukla, S.; Xing, G.; Ge, H.; Prabhakar, R. R.; Mathew, S.; Su, Z.; Nalla, V.; Venkatesan, T.; Mathews, N.; Sritharan, T.; Sum, T. C.; Xiong, Q. Origin of Photocarrier Losses in Iron Pyrite (FeS2) Nanocubes. *ACS Nano* **2016**, *10*, 4431–4440.

(14) Kurmaev, E. Z.; Wilks, R. G.; Moewes, A.; Finkelstein, L. D.; Shamin, S. N.; Kuneš, J. Oxygen x-ray emission and absorption spectra as a probe of the electronic structure of strongly correlated oxides. *Phys. Rev. B* **2008**, *77*, 165127.

(15) Ashcroft, N.; Merimin, N. D. *Solid State Physics*; Saunders College Publishing: New York, 1976.

(16) Nam, S. B.; Reynolds, D. C.; Litton, C. W.; Almassy, R. J.; Collins, T. C.; Wolfe, C. M. Free-exciton energy spectrum in GaAs. *Phys. Rev. B* **1976**, *13*, 761–767.

(17) Sklénard, B.; Dragoni, A.; Triozon, F.; Olevano, V. Optical vs electronic gap of hafnia by *ab initio* Bethe-Salpeter equation. *Appl. Phys. Lett.* **2018**, *113*, 172903.

(18) Jia, J. J.; Callcott, T. A.; Yurkas, J.; Ellis, A. W.; Himpsel, F. J.; Samant, M. G.; Stöhr, J.; Ederer, D. L.; Carlisle, J. A.; Hudson, E. A.; Terminello, L. J.; Shuh, D. K.; Perera, R. C. C. First experimental results from IBM/TENN/TULANE/LLNL/LBL undulator beamline at the advanced light source. *Rev. Sci. Instrum.* **1995**, *66*, 1394–1397.

(19) Regier, T.; Krochak, J.; Sham, T. K.; Hu, Y. F.; Thompson, J.; R, B. R. I. Performance and capabilities of the Canadian Dragon: The SGM beamline at the Canadian Light Source. *Nucl. Instrum. Meth. A* **2007**,

(20) Braun, C.; Seibald, M.; Börger, S.; Oeckler, O.; Boyko, T.; Moewes, A.; Miehe, G.; Tücks, A.; Schnick, W. Material Properties and Structural Characterization of $M_3Si_6O_{12}N_2$:Eu^{2+} (M=Ba, Sr)-A Comprehensive Study on a Promising Green Phosphor for pc-LEDs. *Chem.-Eur. J* **2010**, *16*, 9646–9657.

(21) Schwarz, K.; Blaha, P.; Madsen, G. K. H. Electronic structure Calculations of solids using the WIEN2k package for material sciences. *Comput. Phys. Commun.* **2002**, *147*, 71–76.

(22) Tran, F.; Blaha, P. Accurate Band Gaps of Semiconductors and Insulators with a Semilocal Exchange-Correlation Potential. *Phys. Rev. Lett.* **2009**, *102*, 226401.

(23) Perdew, J. P.; Burke, K.; Ernzerhof, M. Generalized Gradient Approximation Made Simple. *Phys. Rev. Lett.* **1996**, *77*, 3865–3868.

(24) Lengauer, W. Properties of bulk δ-TiN_{1-x} prepared by nitrogen diffusion into titanium metal. *J. Alloys Compd.* **1992**, *186*, 293–307.

(25) Wolf, T. Herstellung und Charakterisierung von TiN, ZrN und HfN. Ph.D. thesis, University of Karlsruhe, 1982.

(26) Smith, D. K.; Newkirk, W. The crystal structure of baddeleyite monoclinic ZrO_2 and its relation to the polymorphism of ZrO_2. *Acta Crystallographica* **1965**, *18*, 983–991.

(27) Ruh, R.; Corfield, P. W. R. Crystal Structure of Monoclinic Hafnia and Comparison with Monoclinic Zirconia. *Journal of the American Ceramic Society* **1970**, *53*, 126–129.